Electronic Supplementary Material (ESI) for Journal of Materials Chemistry A.
This journal is © The Royal Society of Chemistry 2019

Electronic Supplementary Information (ESI)

Direct evidence for two-dimensional oxygen diffusion in the hexagonal perovskite-related oxide $Ba_3MoNbO_{8.5-\delta}$

Masatomo Yashima,*[a] Takafumi Tsujiguchi,[a] Kotaro Fujii,[a] Eiki Niwa,[a] Shunta Nishioka,[a,b] James R. Hester,[c] and Kazuhiko Maeda[a]

a. Department of Chemistry, School of Science, Tokyo Institute of Technology, 2-12-1-W4-17, O-okayama, Meguro-ku, Tokyo, 152-8551, Japan.

b. Japan Society for the Promotion of Science, Kojimachi Business Center Building, 5-3-1, Kojimachi, Chiyoda-ku, Tokyo 102-0083, Japan.

c. Australian Centre for Neutron Scattering, Australian Nuclear Science and Technology Organisation (ANSTO), Locked Bag 2001, Kirrawee DC, NSW, 2232, Australia

* Corresponding author: yashima@cms.titech.ac.jp

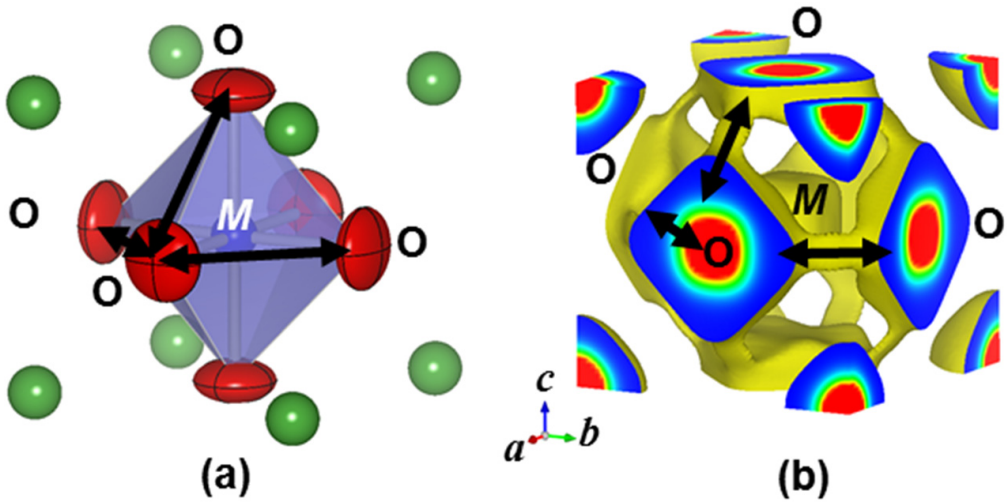

Figure S1. Crystal structure (a) and isosurface of neutron scattering length density (b) of $(La_{0.8}Sr_{0.2})(Ga_{0.8}Mg_{0.15}Co_{0.05})O_{2.8}$ at 1392 °C (Ref. 8). A sintered sample was synthesized by the solid-state reactions. Neutron-diffraction data of the sintered sample was measured *in situ* at 1392 °C in air and then analyzed by Rietveld, MEM and MEM-based pattern fitting analyses. See the details in the literature (Ref. 17). An oxide ion migrates the circular –O–O– diffusion pathways around the M (= $Ga_{0.8}Mg_{0.15}Co_{0.05}$) cation of the AMX_3 perovskite-type oxide (A = $La_{0.8}Sr_{0.2}$ and X = O) as shown by the arrows.

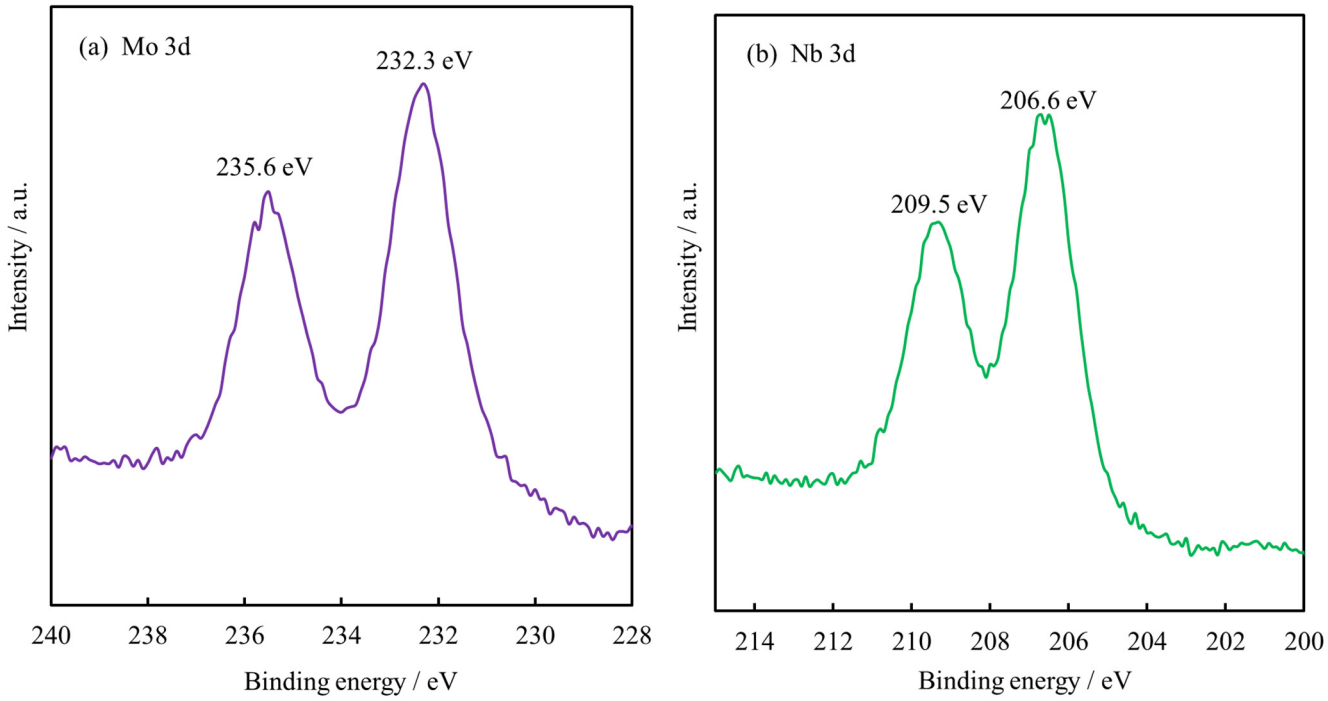

Figure S2. XPS spectra of Mo 3d (a) and Nb 3d (b) in $Ba_3MoNbO_{8.5}$. Two peaks at 232.3 and 235.6 eV in (a) represent the Mo^{6+} $3d_{5/2}$ and Mo^{6+} $3d_{3/2}$ components, respectively. Two peaks at 206.6 and 209.5 eV in (b) represent the Nb^{5+} $3d_{5/2}$ and Nb^{5+} $3d_{3/2}$ components, respectively. Literature[a-f] was referred to for the peak identification.

References

[a] Choi, J.-G., Thompson, L.T. (1996). XPS study of as-prepared and reduced molybdenum oxides. Applied Surface Science 93, 143-149.

[b] Kuepper, K., Balasz, I., Hesse, H., Winiarski, A., Prince, K. C., Matteucci, M., Wett, D., Szargan, R., Burzo, E., Neumann, M. (2004). Electronic and magnetic properties of highly ordered Sr_2FeMoO_6. Physica Status Solidi (a), 201, 3252-3256.

[c] Fleisch, T. H., Mains, G. J. (1982). An XPS study of the UV reduction and photochromism of MoO_3 and WO_3. The Journal of Chemical Physics, 76, 780-786.

[d] Ozer, N., Rubin, M. D., Lampert, C. M. Optical and electrochemical characteristics of niobium oxide films prepared by sol-gel process and magnetron sputtering. A comparison. (1996). Solar Energy Materials and Solar Cells 40, 285-296.

[e] Morris, D., Dou, Y., Rebane, J., Mitchell, C. E. J., Egdell, R. G., Law, D. S. L., et al. (2000). Photoemission and STM study of the electronic structure of Nb-doped TiO_2. Physical Review B, 61, 13445.

[f] Courths, R., Höchst, H., Steiner, P., Hüfner, S. (1980). X-ray and UV photoemission from defects in $LiNbO_3$ and $BaTiO_3$ surfaces. Ferroelectrics, 26, 745-748.

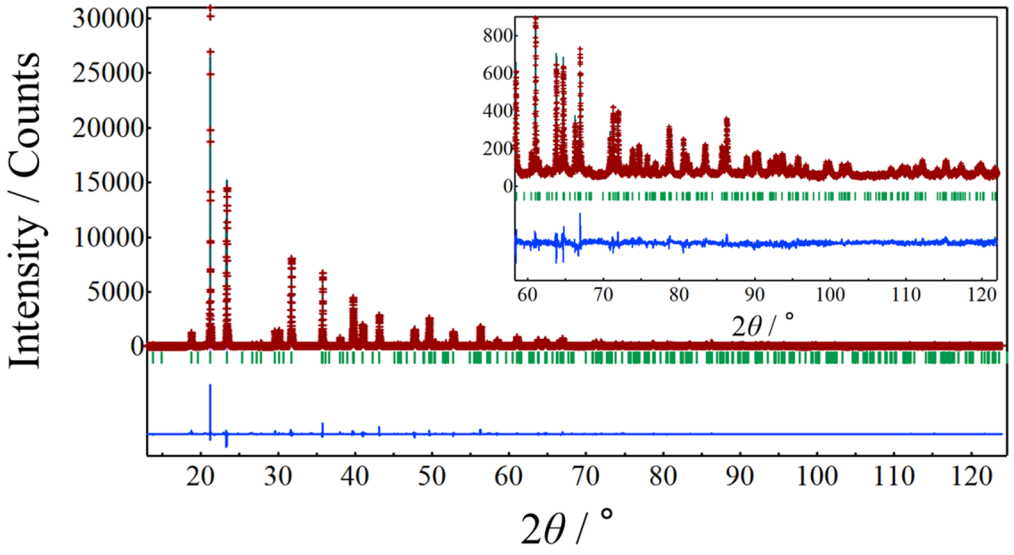

Figure S3. Rietveld pattern of the synchrotron X-ray powder diffraction data of $Ba_3MoNbO_{8.5}$ at 25.6 °C, based on the trigonal $R\bar{3}m$ hybrid structure consisting of 9R polytype and palmierite structures (Fig. 1c). Red crosses and green line denote the observed and calculated intensities, respectively. Green tick marks and blue line below the profile stand for the calculated peak positions and difference pattern, respectively.

Table S1. Refined crystal parameters and reliability factors in Rietveld analysis of neutron diffraction data of $Ba_3MoNbO_{8.5-\delta}$ measured at 21 °C (δ = 0.000(9)).

site label s	atom X	site	x	y	z	$g(X; s)$	U_{eq} or U_{iso}	U_{11} / Å^2	U_{22} / Å^2	U_{33} / Å^2	U_{12} / Å^2	U_{13}/ Å^2	U_{23} / Å^2
Ba1	Ba	3*a*	0	0	0	1	0.0130(16)	0.0173(19)	0.0173(19)	0.004(3)	0.0087(10)	0	0
Ba2	Ba	6*c*	0	0	0.2061(3)	1	0.0220(13)	0.0173(13)	0.0173(13)	0.046(3)	0.0087(6)	0	0
Mo/Nb1	$Mo_{0.5}Nb_{0.5}$	6*c*	0	0	0.39783(17)	0.919(6)	0.0174(11)	0.0098(13)	0.0098(13)	0.046(2)	0.0049(7)	0	0
Mo/Nb2	$Mo_{0.5}Nb_{0.5}$	3*b*	0	0	0.5	0.081(7)	0.0174(11)	0.0098(13)	0.0098(13)	0.046(2)	0.0049(7)	0	0
O1	O	18*h*	0.17278(18)	–0.17278(18)	0.10393(8)	1	0.0209(9)	0.0245(8)	0.0245(8)	0.0210(12)	0.0178(9)	0.0034(5)	–0.0034(5)
O2	O	9*e*	0.5	0	0	0.5	0.0371(16)	0.025(2)	0.058(4)	0.039(4)	0.0289(19)	0.015(2)	0.030(4)
O3	O	36*i*	0.091(2)	0.077(3)	0.3198(5)	0.0833(8)	0.029(4)						

Crystal system: trigonal. Space group: $R\bar{3}m$, Lattice parameters: a = 5.9221(11) Å, c = 21.076(3) Å. $g(X, s)$: Occupancy factor of X atom at the s site. g(Ba, Ba1) = g(Ba, Ba2) = g(O, O1) = 1. U_{ij}: Anisotropic atomic displacement parameter (ADP). $U_{ij} = U_{ij}(s) = U_{ij}(X; s)$: Anisotropic ADP of X atom at the s site. Linear constraints for the anisotropic ADPs: $U_{22}(s1) = U_{11}(s1)$, $U_{12}(s1) = U_{11}(s1)/2$, $U_{13}(s1) = U_{23}(s1) = 0$ for $s1$ = Ba1, Ba2, Mo/Nb1, Mo/Nb2; U_{ij}(Mo/Nb2) = U_{ij}(Mo/Nb1); U_{22}(O1) = U_{11}(O1), U_{13}(O1) = $-U_{23}$(O1); U_{22}(O2) = $2U_{12}$(O2), U_{23}(O2) = $2U_{13}$(O2). U_{eq}: Equivalent isotropic ADP. U_{iso}: Isotropic ADP.

O3–O3 distance on the oxide-ion conducting layer = 0.34(4) Å, O2–O3 distance on the oxide-ion conducting layer = 1.723(17) Å.

Table S2. Refined crystal parameters and reliability factors in Rietveld analysis of neutron diffraction data of $Ba_3MoNbO_{8.5-\delta}$ measured *in situ* at 1100 °C ($\delta = 0.16(3)$).

site label s	atom X	site	x	y	z	$g(X; s)$	U_{eq} or U_{iso}	U_{11} / Å^2	U_{22} / Å^2	U_{33} / Å^2	U_{12} / Å^2	U_{13}/ Å^2	U_{23} / Å^2
Ba1	Ba	3*a*	0	0	0	1	0.064(3)	0.083(5)	0.083(5)	0.026(5)	0.042(3)	0	0
Ba2	Ba	6*c*	0	0	0.2049(4)	1	0.073(3)	0.070(3)	0.070(3)	0.079(6)	0.035(1)	0	0
Mo/Nb1	$Mo_{0.5}Nb_{0.5}$	6*c*	0	0	0.4014(2)	0.973(9)	0.049(2)	0.042(2)	0.042(2)	0.064(4)	0.021(1)	0	0
Mo/Nb2	$Mo_{0.5}Nb_{0.5}$	3*b*	0	0	0.5	0.053(18)	0.049(2)	0.042(2)	0.042(2)	0.064(4)	0.021(1)	0	0
O1	O	18*h*	0.1748(3)	–0.1748(3)	0.10185(13)	1	0.077(2)	0.093(2)	0.093(2)	0.076(3)	0.070(2)	0.0051(11)	–0.0051(11)
O2	O	9*e*	0.5	0	0	0.343(6)	0.139(7)	0.1118(6)	0.26(2)	0.086(13)	0.131(4)	0.036(8)	0.073(9)
O3	O	36*i*	0.094(2)	0.080(4)	0.3229(5)	0.1095(9)	0.050(5)						

Crystal system: trigonal. Space group: $R\bar{3}m$, Lattice parameters: a = 6.0914(4) Å, c = 21.3710(13) Å. $g(X, s)$: Occupancy factor of X atom at the s site. g(Ba, Ba1) = g(Ba, Ba2) = g(O, O1) = 1. U_{ij}: Anisotropic atomic displacement parameter (ADP). $U_{ij} = U_{ij}(s) = U_{ij}(X; s)$: Anisotropic ADP of X atom at the s site. Linear constraints for the anisotropic ADPs: $U_{22}(s1) = U_{11}(s1)$, $U_{12}(s1) = U_{11}(s1)/2$, $U_{13}(s1) = U_{23}(s1) = 0$ for $s1$ = Ba1, Ba2, Mo/Nb1, Mo/Nb2; U_{ij}(Mo/Nb2) = U_{ij}(Mo/Nb1); U_{22}(O1) = U_{11}(O1), U_{13}(O1) = $-U_{23}$(O1); U_{22}(O2) = $2U_{12}$(O2), U_{23}(O2) = $2U_{13}$(O2). U_{eq}: Equivalent isotropic ADP. U_{iso}: Isotropic ADP.

O3–O3 distance on the oxide-ion conducting layer = 0.66(4) Å, O2–O3 distance on the oxide-ion conducting layer = 1.39(3) Å.

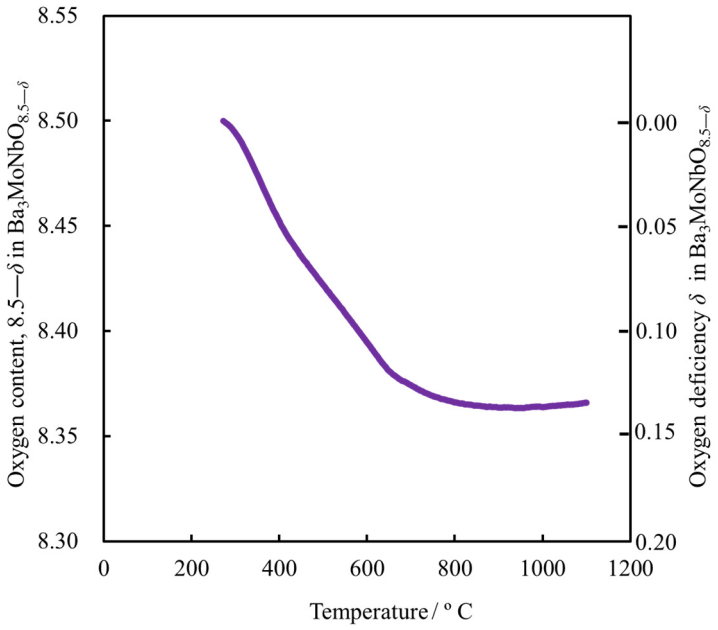

Figure S4. Temperature dependence of the oxygen content 8.5–δ and oxygen vacancy concentration δ of $Ba_3MoNbO_{8.5-\delta}$ in air. These data were obtained by TG measurements.

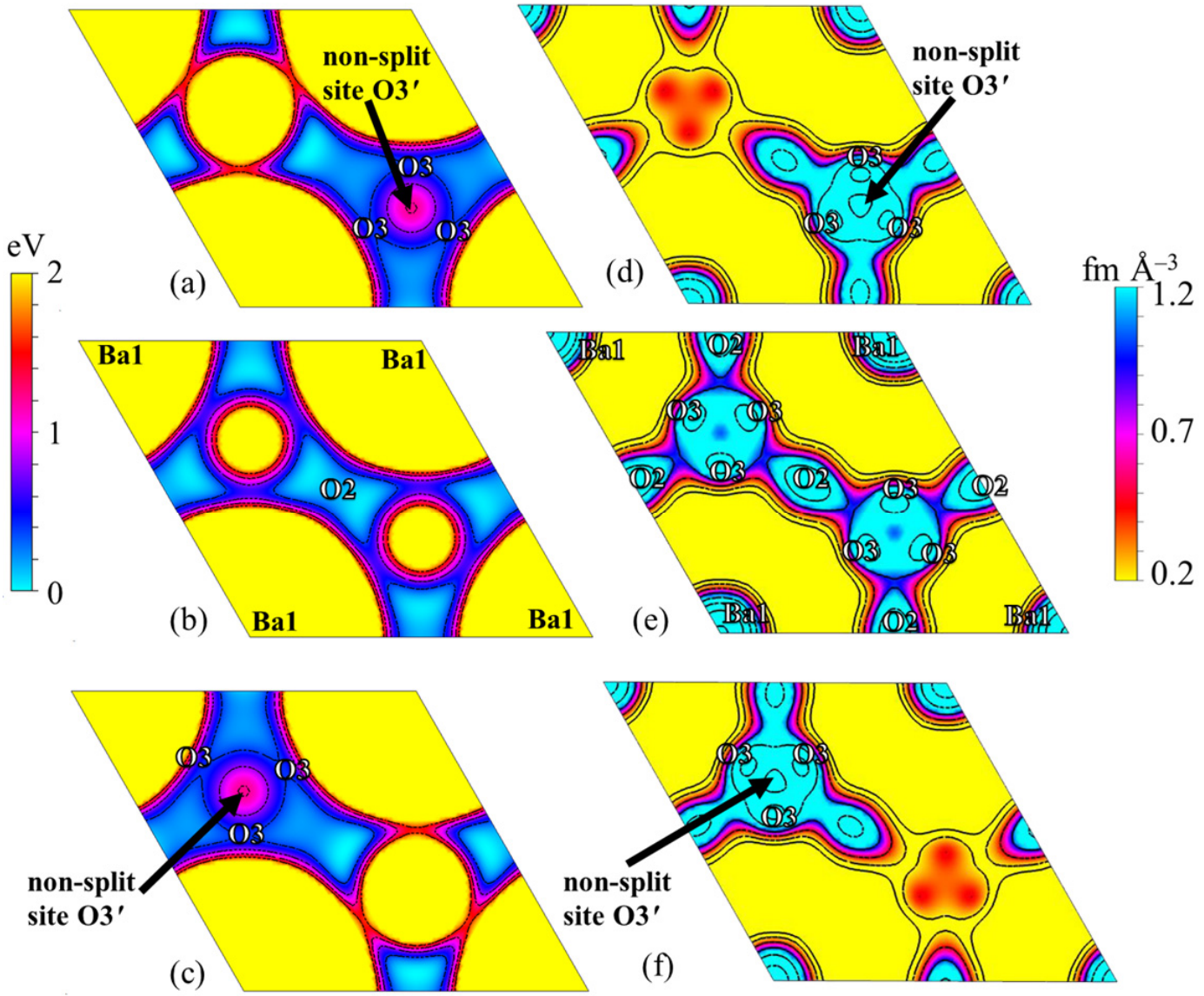

Figure S5. (a-c) Bond-valence-based energy landscapes (BVELs) for a test oxide ion on the *ab* planes at (a) $z = 0.01$, (b) $z = 0$ and (c) $z = –0.01$ in $Ba_3MoNbO_{8.5–\delta}$, which were calculated for the crystal parameters refined using the neutron-diffraction data of $Ba_3MoNbO_{8.5–\delta}$ at 1100 °C ($\delta = 0.16(3)$). (d-g) Corresponding MEM neutron scattering length density (NSLD) distributions on the *ab* planes at (d) $z = 0.01$, (e) $z = 0$ and (f) $z = –0.01$ in $Ba_3MoNbO_{8.5–\delta}$, which were obtained using the neutron-diffraction data of $Ba_3MoNbO_{8.5–\delta}$ at 1100 °C ($\delta = 0.16(3)$). The NSLD distributions are consistent with BVELs. The central position of the tetrahedral oxygen (non-split site O3′) is unstable due to the shorter (Mo/Nb1)–O3′ bond lengths, which is confirmed by the BVELs. The split site O3 is more stable due to the longer (Mo/Nb1)–O3 bond lengths, which is also supported by the BVELs and MEM NSLD distributions.

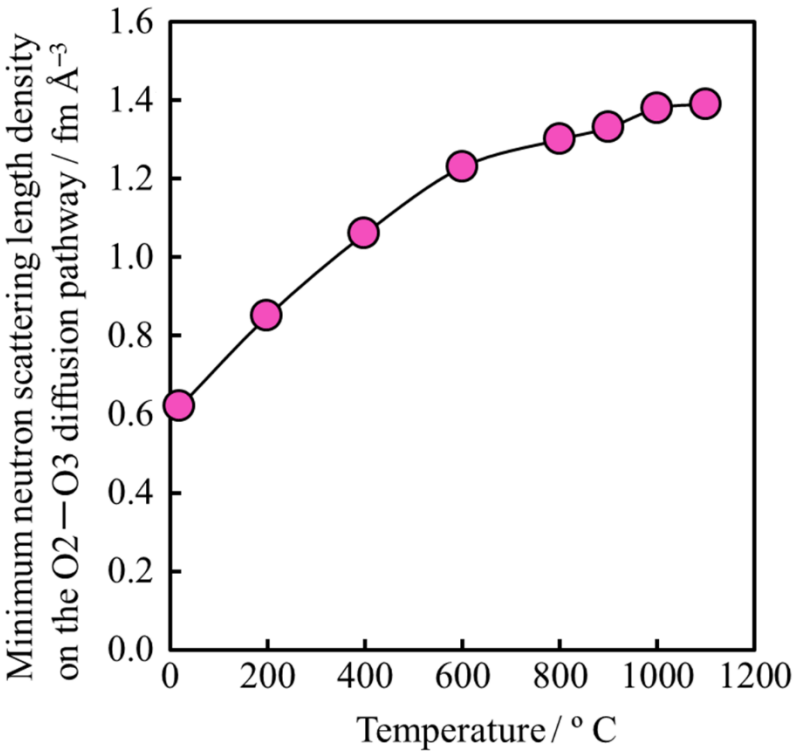

Figure S6. Temperature dependence of minimum neutron scattering length density (NSLD) in the –O2–O3– pathway of $Ba_3MoNbO_{8.5-\delta}$. The minimum NSLD increases with an increase of temperature.

End of the Electronic Supplementary Information ESI.